Journal of Applied Physics

Deep level transient spectroscopy investigation of ultra-wide bandgap (201) and (001) β-Ga_2O_3

Cite as: J. Appl. Phys. **128**, 205701 (2020); https://doi.org/10.1063/5.0021859
Submitted: 15 July 2020 . Accepted: 29 October 2020 . Published Online: 23 November 2020

Jossue Montes, Cameron Kopas, Hong Chen, Xuanqi Huang, Tsung-han Yang, Kai Fu, Chen Yang, Jingan Zhou, Xin Qi, Houqiang Fu, and Yuji Zhao

Journal of Applied Physics ARTICLE scitation.org/journal/jap

Deep level transient spectroscopy investigation of ultra-wide bandgap ($\bar{2}01$) and (001) β-Ga_2O_3

Cite as: J. Appl. Phys. **128**, 205701 (2020); doi: 10.1063/5.0021859
Submitted: 15 July 2020 · Accepted: 29 October 2020 ·
Published Online: 23 November 2020

Jossue Montes,[1] Cameron Kopas,[1] Hong Chen,[1] Xuanqi Huang,[1] Tsung-han Yang,[1] Kai Fu,[1] Chen Yang,[1] Jingan Zhou,[1] Xin Qi,[1] Houqiang Fu,[2] and Yuji Zhao[1,a)]

AFFILIATIONS

[1]School of Electrical, Computer and Energy Engineering, Arizona State University, Tempe, Arizona 85287, USA
[2]Department of Electrical and Computer Engineering, Iowa State University, Ames, Iowa 50011, USA

[a)]**Author to whom correspondence should be addressed:** yuji.zhao@asu.edu

ABSTRACT

This work reports on a comprehensive examination of the electrical and thermal properties of vertical Schottky diodes fabricated on ($\bar{2}01$)- and (001)-oriented samples of β-Ga_2O_3. The temperature-dependent current–voltage (I–V) and capacitance–voltage (C–V) data were gathered and analyzed down to 60 K. Deep level transient spectroscopy (DLTS) was used to study bulk and interface defects in the two materials from approx. 325 K down to 60 K. In the bulk ($\bar{2}01$) material, an electron trap was observed at E_C−0.46 eV, with a capture cross section of 1.6×10^{-14} cm^2 and a lambda-corrected maximum trap density of 9.08×10^{15} cm^{-3}. These results and others indicate that the electron trap is a strong candidate for the well-known *E1* defect in β-Ga_2O_3 based on recent investigations. Additionally, in the ($\bar{2}01$) material, the smooth modulation typical of interface states is evident at temperatures below 275 K. The (001) samples manifested what is likely the *E2** electron trap at E_C−0.68 eV, with a capture cross section of 1.64×10^{-15} cm^2 and a lambda-corrected maximum trap density of 8.85×10^{15} cm^{-3}. The presence of the *E2** defect, in particular, is a contrast to the findings of recent DLTS investigations on β-Ga_2O_3, which report that *E2** emerged only after low-energy proton irradiation. These results help to further map out the defect signatures found in β-Ga_2O_3 materials, which are of vital importance in the design and fabrication of future β-Ga_2O_3 devices.

INTRODUCTION

Beta-phase gallium oxide (β-Ga_2O_3) has enjoyed a resurgence in research interest over the past several years. This interest stems from a number of its material properties: the ultra-wide bandgap of 4.6–4.9 eV; a widely tunable n-type conductivity range between 10^{16} and 10^{19} cm^{-3}; a high theoretical breakdown field of 8 MV/cm; a high electron saturation velocity of 2×10^7 cm/s; a large Baliga's Figure of Merit (BFOM) of 3444 $\epsilon\mu E_c^3$; and the availability of large high-quality single-crystal substrates.[1] In particular, the ultra-wide bandgap enables deep ultraviolet (DUV), high-power applications, and harsh-environment applications, i.e., operating under ionizing radiation. The β-Ga_2O_3 crystal structure is in the C2/m space group, with lattice constants $a = 1.22$ nm, $b = 0.303$ nm, $c = 0.580$ nm, and angle $\beta = 103.8°$.[1,2] The result of this arrangement is a strong cleavage plane parallel to the (100) surfaces, which allows for a simple facile cleavage and a mechanical exfoliation of thin flakes that may be transferred to any arbitrary substrate. This mechanical exfoliation of β-Ga_2O_3, similar to that of other 2D materials such as graphene and the transition metal dichalcogenides, has resulted in a wide range of novel device studies.[3–5]

In order to realize more efficient and varied devices on the relatively nascent β-Ga_2O_3 material platform, a deeper understanding of localized electronic states throughout the bandgap is necessary. Several deep level defects associated with the emission and capture throughout the forbidden band, commonly labeled electron traps *E1* (E_C−0.56 eV), *E2** (E_C−0.75 eV), *E2* (E_C−0.78 eV), and *E3* (E_C−1.01 eV),[6–9] and others have been investigated through various studies using deep level transient spectroscopy (DLTS), among other methods.[10,11] Notably, the defect *E2* is currently believed to be associated with the substitutional defect Fe_{Ga}.[7] *E3* has been proposed to correspond to a substitutional defect Ti_{GaII}, common in commercially available β-Ga_2O_3. The Ti impurity in β-Ga_2O_3 has been suggested for use in quantum information applications.[12,13] Further study and understanding of the nature of these and other β-Ga_2O_3 defects will enable further advancement in these and other technologies.

In this paper, we provide a comprehensive characterization study, using a combination of electrical [I–V, C–V)] and thermal (deep level transient spectroscopy—DLTS) testing on two orientations of β-Ga_2O_3 grown by different methods: the edge-defined film-fed growth (EFG) and hydride vapor-phase epitaxy (HVPE) methods. The planar orientations are ($\bar{2}01$) for the bulk sample and (001) for the epitaxial sample. By varying the DLTS testing setup conditions, particularly the filling and emitting pulses, pulse widths, and frequency ranges, the $E1$ defect is observed in the ($\bar{2}01$) bulk sample for the first time. The $E2^*$ defect is observed in the HVPE sample without any proton irradiation treatment applied. In addition, the effects of interface states between the Schottky contact and β-Ga_2O_3 semiconductor are observed in the DLTS spectra of both materials.

Whereas shallow energy levels in a semiconductor generally arise due to the intentional doping of a certain impurity, deep levels lie farther within the forbidden band and generally arise from the inevitable crystal lattice imperfections such as vacancies, interstitials, contamination, and defect complexes. These defect levels can be introduced during the various thermal growth methods. Whether deep energy levels occur by accident or by design, they can have profound effects on the properties of the semiconductor material and any resulting devices. Notably, they act as carrier traps and can reduce the recombination lifetime of carriers as well as having other effects (e.g., Femi-level effects, diffusion potentials, and material conductivity). Describing these so-called "trap" levels is one of the main purposes of DLTS.

DLTS can be performed on any device capable of forming a depletion region, e.g., MOSCAPs, MOSFETs, and diodes. In this work, DLTS is performed on Schottky diodes. For an n-type material held under constant reverse bias V_R (often called the quiescent bias), a trap state of energy E_T is empty at all energies above the Fermi energy, and there is a relatively wide depletion region (Fig. 1). Charge neutrality demands that the applied negative charges on the metal be compensated by the localized positive charges of the depletion region. A brief, positive pulse V_1 is applied, which results in

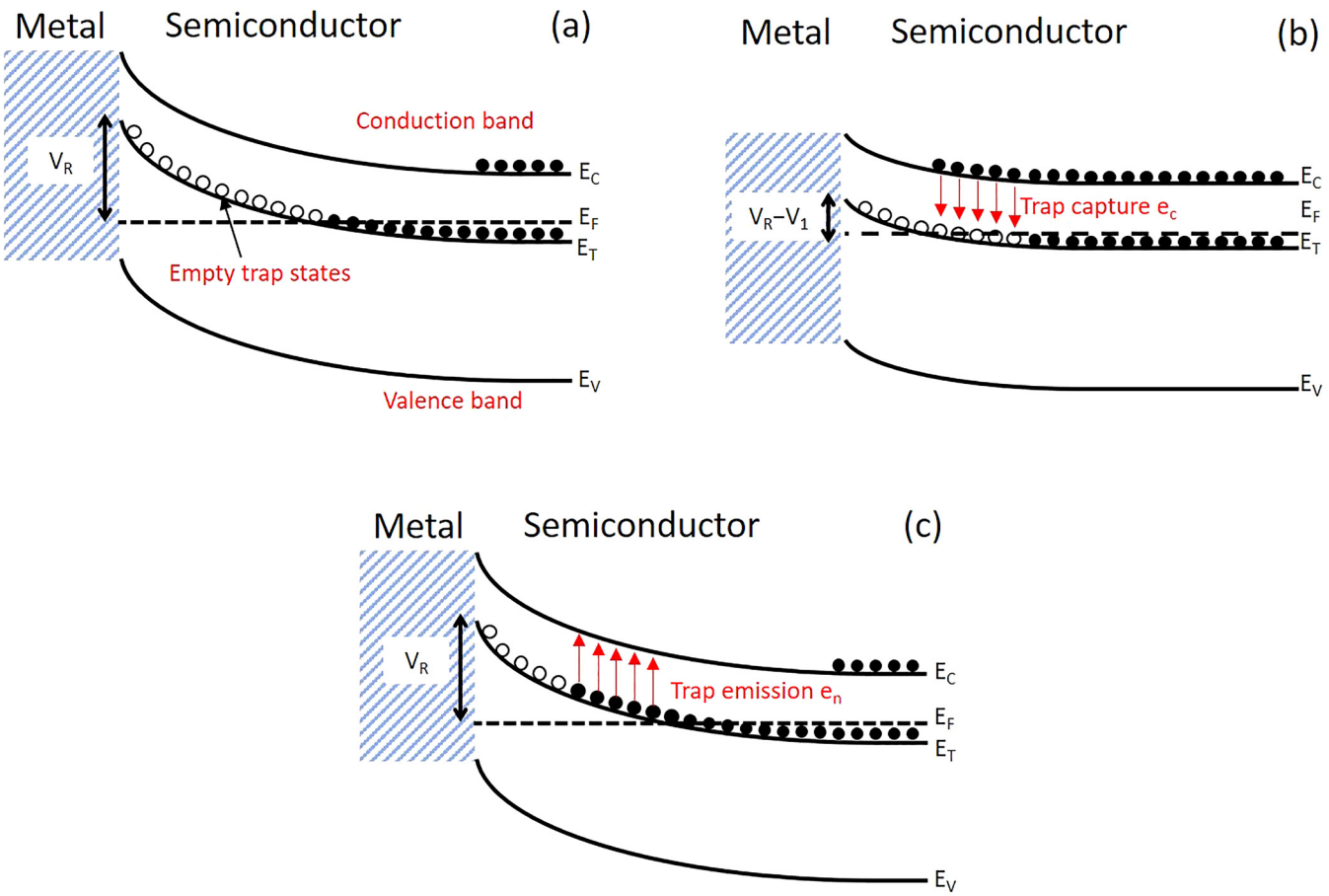

FIG. 1. Thermal capture and emission of electrons in an n-type material. (a) The diode is held under constant reverse bias V_R, with trap states near the interface empty. (b) A positive filling pulse V_1 is applied, capturing conduction band electrons into trap states. (c) After the filling pulse is over, the filled trap states emit electrons back to the conduction band.

trap states below the Fermi energy capturing conduction band electrons. Typical lengths for this filling pulse span from microseconds to tens of seconds.[14] During the filling pulse, the width of the depletion region decreases, which results in a sharp rise in the capacitance of the junction. When the filling pulse expires, the trap level emits electrons back to the conduction band. The depletion region re-widens to its original value, restoring the capacitance, albeit with an exponential transient due to the emission of trapped carriers.

Deep levels emit trapped carriers via thermal emission. They capture carriers via the opposite process, and the two processes are related via the detailed balance relation

$$e_n = \frac{g_0}{g_1} \nu_{th} \sigma_n N_C \exp\left(-\frac{E_C - E_T}{kT}\right), \tag{1}$$

where e_n is the electron thermal emission rate, ν_{th} is the thermal velocity, σ_n is the capture cross section for electrons, N_C is the electron density of states, g_0/g_1 is the ratio of the degeneracy of empty and occupied states, and E_T is the energy level of the deep level under scrutiny. The rest of the terms carry the usual definitions. Recalling the free carrier concentration, $n = N_C \exp((E_F - E_T)/kT)$, and assuming a degeneracy ratio of 1, the emission rate e_n can be expressed as

$$e_n = \nu_{th} \sigma_n \exp\left(-\frac{E_F - E_T}{kT}\right). \tag{2}$$

Recalling the Maxwell–Boltzmann velocity distribution, the thermal velocity $\nu_{th} = (3kT/m_{eff})^{1/2}$, and the effective density of states for electrons $N_C = 2(2\pi m_{eff} kT/h^2)^{3/2}$, we can rewrite the emission rate as

$$e_n = 2(3)^{1/2} k^2 m_{eff} \left(\frac{2\pi}{h^2}\right)^{\frac{3}{2}} T^2 \sigma_n \exp\left(-\frac{E_C - E_T}{kT}\right). \tag{3}$$

We can group the non-temperature-dependent constants together as α and take the natural log of the resulting equation to get the famous Arrhenius relation

$$In\left(\frac{e_n}{T^2}\right) = \ln(\sigma_n \alpha) - \left(\frac{E_C - E_T}{kT}\right). \tag{4}$$

It should be noted that σ_n is frequently assumed to be temperature independent and collected as a constant. The corresponding Arrhenius plot can be derived by collecting emission data as a function of temperature, which is done during the DLTS measurement. The dependence of the emission rate e_n on temperature T is derived from a series of DLTS spectra for different pulse frequencies, widths, and amplitudes, thus characterizing an electrically active defect's density N_T, capture cross section σ, and bandgap energy E_T. As the capture and emission of carriers is an exponential process, the two have their respective time constants: $\tau_e = 1/e_n$ for emission and $\tau_c = (\sigma_n \nu_{th} n)^{-1}$ for capture. The ratio of the two time constants, namely, $\tau_c/\tau_e = \exp(E_T - E_F)/kT$, again reaffirms that for trap levels above the Fermi energy, the capture process dominates.

EXPERIMENTAL

Two 2-in. substrates of β-Ga_2O_3 were obtained from Tamura Corporation. The first was an unintentionally doped (UID) ($N_D - N_A \approx 1$–$4 \times 10^{16}\,cm^{-3}$) epi-wafer grown by HVPE on a Sn-doped ($N_D - N_A \approx 1$–$20 \times 10^{18}\,cm^{-3}$) substrate. The thickness of the UID epilayer is 10 μm, and the thickness of the substrate is 640 μm ± 20 μm. The second 2-in. substrate was a Sn-doped ($N_D - N_A = 5.5 \times 10^{18}\,cm^{-3}$) ($\bar{2}01$) single-crystal substrate grown by the EFG method. Both substrates were cleaved into small $1 \times 1.5\,cm^2$ samples. Each sample was cleaned in an ultrasonic wash for 5 min using acetone, followed by IPA, and then air-dried in N_2. Large-area backside ohmic contacts of Ti/Al/Ti/Au (20 nm/130 nm/20 nm/50 nm) were deposited using e-beam evaporation and subsequently annealed in N_2 ambient at 470 °C for 1 min. Prior to the ohmic contact deposition, the backside was treated by a BCl_3/Ar plasma etch for 5 min to facilitate the formation of ohmic contacts.[15] The ICP source power was 400 W, and the bias power was 30 W. At a BCl_3/Ar flow rate of 20/5 sccm and a pressure of 15 mTorr, the etch rate was approx. 20 nm/min. The sample was cleaned again after the ohmic contact deposition. Standard photolithography using positive photoresists (LOR3A and AZ3312) was used to pattern and expose the 600-μm diameter Schottky contacts. The Schottky contacts consisted of Ni/Au (150 nm/200 nm) stacks.[16]

Electrical characterization of the Schottky diodes of both samples was performed using standard current–voltage (I–V) and capacitance–voltage (C–V) tests. To facilitate ease of testing, separate diodes with slightly lower doping ($N_D - N_A = 8.7 \times 10^{17}\,cm^{-3}$), but identical fabrication, were used for electrical testing vs the thermal testing. The I–V tests were carried out using an HP-4140B DC source/picoammeter, while the C–V tests were carried out using a DLS-83D Deep Level Spectrometer. The sample temperature was controlled using a Lakeshore 331 Temperature Controller and a CTI-Cryogenics Model 21 Refrigerator. This hardware allows for temperatures between approx. 30 K and 325 K as well as a controllable temperature ramp rate for the DLTS. The DLTS investigation was carried out using a DLS-83D Deep Level Spectrometer from Semilab. The cryogenic chamber housing the samples was made by Janis Research Company (Serial No. 20903). In this implementation, the DLTS signal is measured by a Lock-in Integrator set to the corresponding measurement frequency (or rate window), with a 3 s integration time constant to minimize noise. This implementation, also known as constant voltage DLTS, uses a feedback loop to measure the capacitance transients that arise from the filling pulses (V_1). The temperature ramp rate was set to −100 mK/s for all measurements, to take into account the relatively poor thermal conductivity of β-Ga_2O_3. For the $\bar{2}01$ β-Ga_2O_3 sample, the DLTS study used a reverse bias $V_R = -0.4$ V and filling pulse $V_1 = 0.1$ V with pulse widths set to 20 μs. Measurements at lower frequencies and higher reverse and filling pulse biases did not find additional defect activity. For the HVPE (001) sample, the study was carried out across a varying frequency between 1 and 4 Hz. The filling pulse width in all cases was 10 ms. This optimum frequency range and pulse width yielded more meaningful data compared to the range used with the EFG sample. The reverse bias V_R was −6 V and the filling pulse V_1 was 1 V with identical pulse widths (20 μs).

RESULTS AND DISCUSSION

The relevant diode electrical parameters, e.g., diode ideality factors, Schottky barrier heights, and carrier concentrations, are presented in Figs. 2 and 3. The carrier concentrations calculated from the A/C^2 data match well with the commercial vendor specifications. Notably, approaching room temperature, the diodes exhibit an ideality factor close to unity, indicating band-to-band recombination, whereas $n = 2$ corresponds to defect-assisted Shockley–Read–Hall (SRH) recombination. This latter recombination is markedly increased for the heavily doped ($\bar{2}01$) sample compared to the UID (001) sample across the temperature region studied, indicating defects are far more electrically active in the heavily doped, bulk-growth material.

The DLTS spectra for the $\bar{2}01$ sample, split into two temperature regions, are shown in Fig. 4. At temperatures below 200 K, there are broad, smooth extrema visible, which likely correspond to interface states between the semiconductor and the metal.[17] While bulk defects occupy a single discrete energy level in the bandgap, interface states occupy a continuum of energy levels, though emission from energies interface traps in the upper portion of the bandgap will dominate. In Fig. 4(b), we observe a majority carrier (electron) defect between 225 and 250 K with energy 0.46 eV below the conduction band. Based on the changing amplitudes of the DLTS signal, a varying trap concentration can be deduced. This situation has been observed in previous works[9,18] and can arise for defect complexes or defect minibands.[19,20] Such a situation may arise in the β-Ga_2O_3 samples under study due to the prevalence of surface states, evident in Fig. 1(a) and discussed later on. The maximum trap density, N_T, for this defect in the $\bar{2}01$ sample was

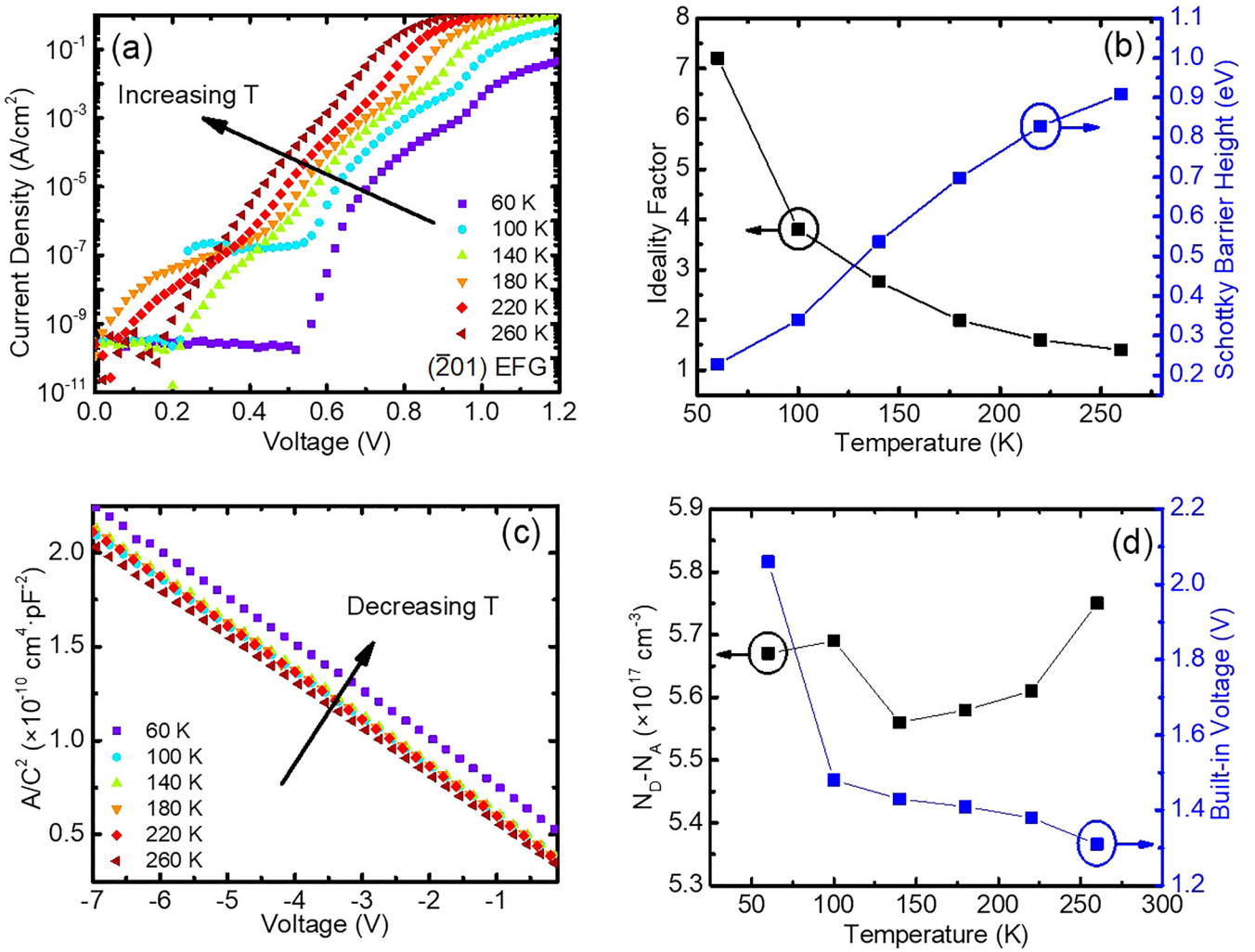

FIG. 2. Temperature-dependent electrical data from the EFG ($\bar{2}01$) sample. (a) Forward current density data. (b) Ideality factor and Schottky barrier height, as determined from *I–V* data. (c) A/C^2 plot, as determined from *C–V* data. (d) Doping concentration and built-in voltage, determined from both *I–V* and *C–V* data.

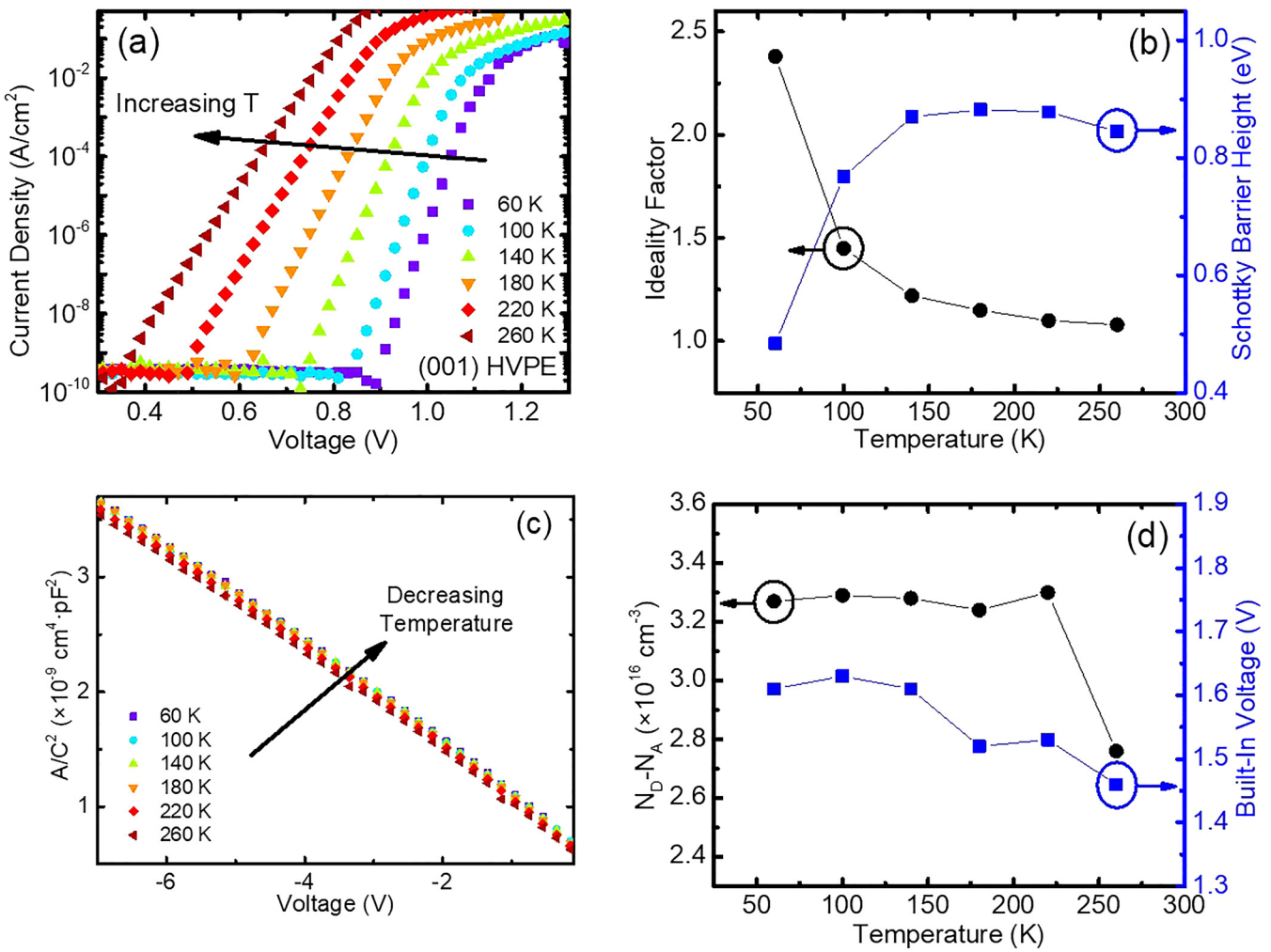

FIG. 3. Temperature-dependent electrical data from the HVPE (001) sample. (a) Forward current density data. (b) Ideality factor and Schottky barrier height, as determined from *I–V* data. (c) A/C^2 plot, as determined from *C–V* data. (d) Doping concentration and built-in voltage, determined from both *I–V* and *C–V* data.

9.08×10^{15} cm^{-3} over the temperature range where peaks occurred. The lambda effect correction was applied to N_T.[19,20] As the frequency is increased, the defect can be seen activating at progressively higher temperatures.

The defect often referred to as *E2* in β-Ga_2O_3 (typically 0.78 eV below CBM, and thought to correspond to a Ga vacancy) typically exhibits a peak emission response at $T \sim 360$ K.[7] This temperature is outside the maximum range for our DLTS cryostat; however, in the $(\bar{2}01)$ β-Ga_2O_3 sample, we observe the "tail" of a majority carrier peak with high DLS signal intensity almost certainly corresponding to *E2*. We are unable to further characterize this defect, but a closer examination of this is shown in Fig. 5.

The associated DLTS spectra for the HVPE (001) sample are shown in Fig. 6. A defect can be clearly identified around the temperature 325 K (energy 0.68 eV below the conduction band and lambda-corrected maximum $N_T = 8.85 \times 10^{15}$ cm^{-3}), and the tail for the *E2* defect again can be observed outside the temperature testing range [Fig. 6(b)]. Once again, at higher frequencies, the defect's peak response shifts slightly higher in temperature. While the 1–3 Hz scans do not reveal any notable activity below approx. 275 K, the 4 Hz scan distinctly shows some smooth interface state activity below 275 K.

The DLTS signal intensities observed in the (001) β-Ga_2O_3 epilayers grown by HVPE are lower compared to the intensities in the $(\bar{2}01)$ β-Ga_2O_3 crystals grown by EFG. This is consistent with the lower nominal doping concentration and lower ideality factors measured by *I–V* (Figs. 2 and 3) as well as with recent studies comparing epitaxially grown β-Ga_2O_3 vs bulk methods.[7,8] The resulting Arrhenius plot and relevant DLTS parameters from the frequency spectra in Figs. 4 and 6 can be seen in Fig. 7. The peak

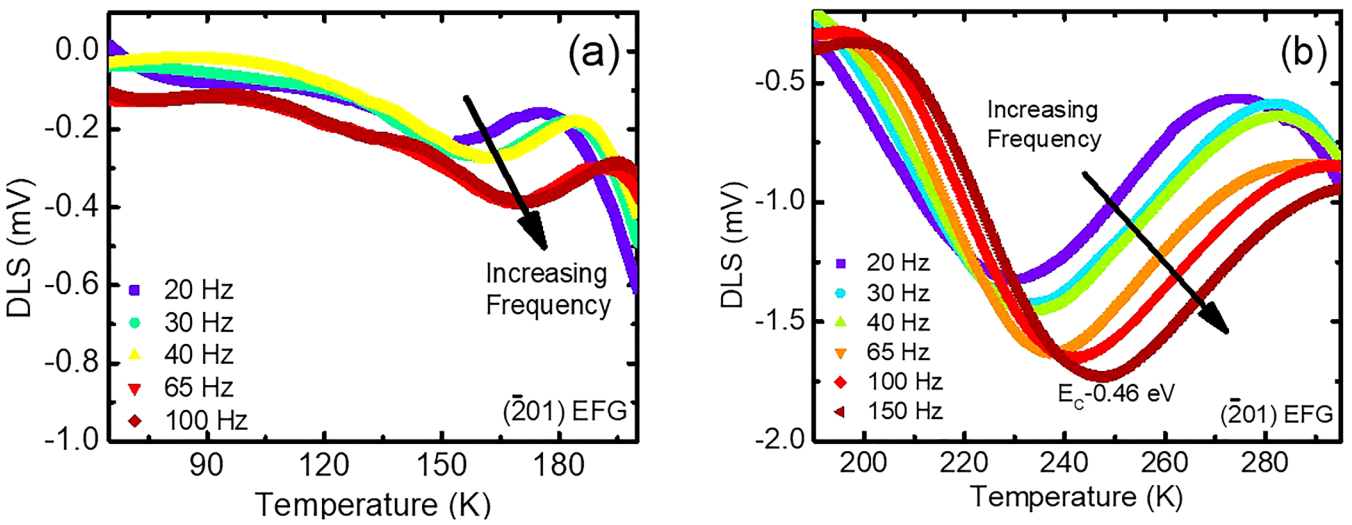

FIG. 4. DLTS data obtained from ($\bar{2}01$) β-Ga_2O_3 crystals grown by EFG. Measurements performed with: quiescent reverse bias $V_R = -0.4$ V; pulse voltage $V_1 = 0.1$ V; pulse width = 20 μs; temperature ramp rate = −100 mK/s. (a) DLTS data from 75 to 200 K. (b) DLTS data from 180 to 300 K. Note the vertical scale difference of the two regions.

emission rate, e_n, is 5.98×10^7 s·K^2 for the EFG ($\bar{2}01$) defect and 4.54×10^9 s·K^2 for the HVPE (001) defect. We can also calculate the capture time constant τ_c as 3.28×10^{-16} s^{-1} for the EFG ($\bar{2}01$) sample and 5.96×10^{-13} s^{-1} for the HVPE (001) sample.

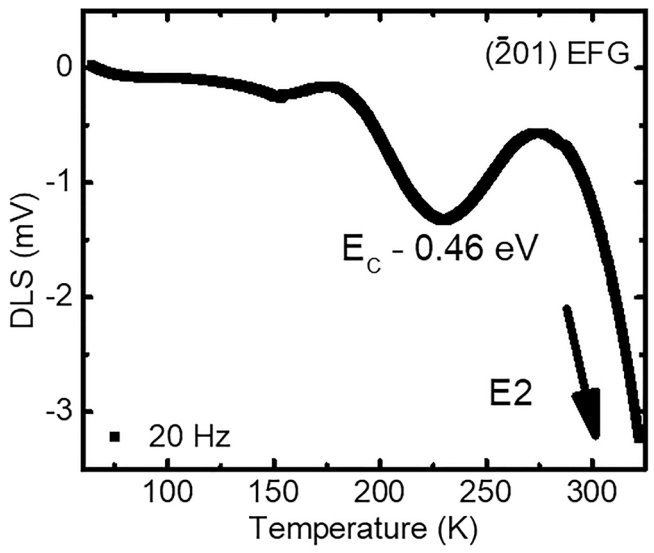

FIG. 5. DLTS data obtained from ($\bar{2}01$) β-Ga_2O_3 crystals grown by EFG. Measurement performed with: quiescent reverse bias $V_R = -0.4$ V; pulse voltage $V_1 = 0.1$ V; pulse width = 20 μs; temperature ramp rate = −100 mK/s. This scan was taken out to a higher temperature, showing the low-temperature side of the prominent *E2* defect present in all β-Ga_2O_3 materials.

Upon examining the defect labeled in Fig. 4(b) and considering its activation temperature, energy placement, capture cross section, and trap density, one could reasonably conclude that this defect is likely the *E1* defect based on the summary information in Table I. Prior to this study, *E1* has only been observed in epitaxially grown β-Ga_2O_3 materials.[7–10] We observe the *E1* defect lying at E_C−0.46 eV in the ($\bar{2}01$) bulk sample, occurring at approx. the same temperature region (230–250 K) as the aforementioned studies. The lack of response to irradiation[8] and the general omnipresence of *E1* in many studies and growth methods would indicate that the defect is related to impurities. Remarkably, Ingebrigtsen *et al.* demonstrated that bulk and epitaxial wafers [EFG (010), molecular beam epitaxy (MBE) (010), and HVPE (001)] manifest the *E1* defect at nearly the exact same energy (E_C−0.56 eV) and capture cross section ($0.3–5 \times 10^{-13}$ cm^2) across several studies. Others have found comparable energies for *E1*, though trap densities and capture cross sections vary up to two orders of magnitude (Table I). These inconsistencies may be a consequence of different test settings and device fabrication. Materials grown by bulk growth methods such as Czochralski and EFG typically exhibit higher trap densities for *E1* and other defects. It has been suggested[21–25] that the electron trap *E1* may be due to Fe or Co impurities, possibly incorporated during the growth process.

For the (001) HVPE sample, there is excellent agreement in activation temperatures (325 K) and reasonable overlap in the bandgap position between this study and the *E2** defect cited by others.[8,9] Furthermore, the defect *E2** has a rather characteristic placement in the spectrum, riding the low-temperature shoulder of the prominent *E2* defect.[8] These remarkable similarities would lead one to suspect that the defect in Figs. 6(a) and 7 is *E2**; however, *E2** has hitherto been detected only after low-energy (600 keV … 1 MeV)[7,8] proton irradiation was applied. Polyakov

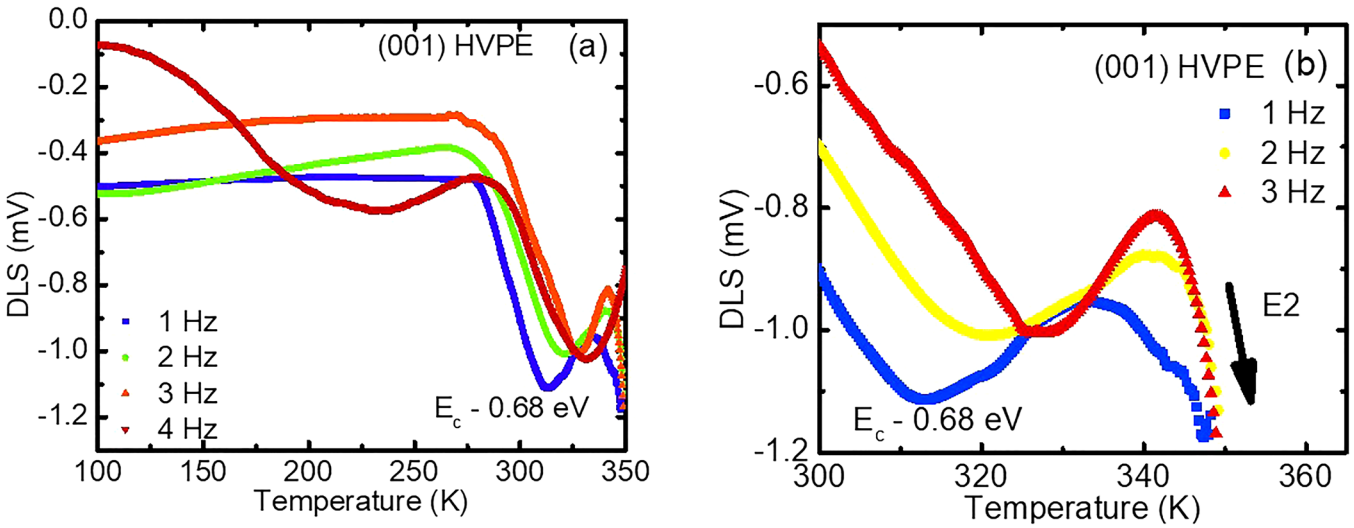

FIG. 6. DLTS data obtained from (001) β-Ga_2O_3 epilayers grown by HVPE. Measurement settings are quiescent reverse bias $V_R = -6$ V; pulse voltage $V_1 = 1$ V; pulse width = 10 ms; temperature ramp rate = −100 mK/s. (a) DLTS data for the 100–350 K temperature region. The 4 Hz scan shows the distinct smooth modulation typical of interface while the others do not, which we attribute to detection thresholds. (b) The 300–350 K temperature region magnified, showing the front "tail" end of the E2 defect.

et al. did not observe the defect at all after high energy (10 MeV) proton irradiation was applied.[14] These inconsistencies may be due to any number of differences in testing setups and sample preparation. Regardless, the E_C−0.46 eV defect visible in Fig. 6(a) seems to be a prime candidate for *E2** designation in spite of no proton irradiation occurring in this study. The exact origin of *E2** has been suggested to be V_{Ga} or complexes thereof, as its signature has

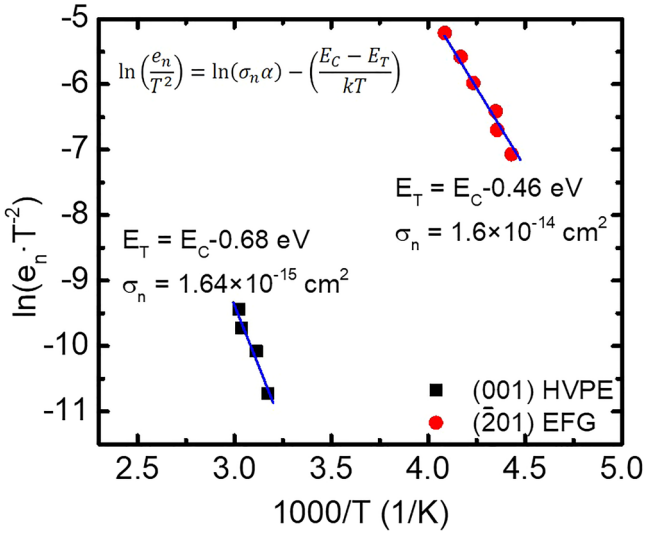

FIG. 7. Arrhenius plot for the EFG-grown ($\bar{2}01$) and HVPE-grown (001) samples. The electron effective mass used is $0.28m_0$.

appeared in bulk EFG (010) and epitaxial HVPE (001), MBE (010) samples post-irradiation (Table I). This study revealed what is likely the *E2** defect in the absence of any radiation treatments. It is possible that the annealing step in the fabrication of our Schottky diodes may have been the thermal treatment catalyst for a weak *E2** signal to appear. Whatever the case, *E2** is regarded as an intrinsic defect or a complex involving intrinsic elements. The electron trap *E2* (different from *E2**) is an ubiquitous finding in essentially every DLTS study performed to date on β-Ga_2O_3, though it was not considered in this study. Several recent studies employing secondary ion mass spectrometry (SIMS) have assigned *E2* to be from a Fe_{Ga} substitution, with some preference to the octahedral Ga sites.[6] Bulk growth methods, such as Czochralski and EFG (this study), often require the use of an Ir crucible, where contamination from Ir and residual Fe is likely. Epitaxial growth methods, e.g., MBE and HVPE (this study), do not require an Ir crucible and will naturally have less Fe contamination, again consistent with this study.

The electrical activity of surface states is evident in Figs. 4(a) and 6(a). Surface states have long been understood to be a detriment to the fabrication of successful semiconductor devices.[2,16] For DLTS studies, surface states compete with bulk defects during the capture and emission process. The net result is a decreased signal in the various spectra. In order to quantify the dynamics of these two competing mechanisms, further investigations such as admittance spectroscopy (AS) must be done.[11] The doping concentration as a function of depletion region width is shown in Fig. 8. Based on the widths, we can assume that the surface states do not have a significant role in the DLTS experiments here.

Besides interface states, leaky devices tend to also suffer noise in their DLTS spectra.[26] This is owed to a competition between the thermal capture of trapped carriers vs electrical capture due to

TABLE I. Summary of relevant DLTS studies on β-Ga_2O_3. Units for numerical quantities are as follows: E_{CT} (eV); σ_n ($\times 10^{-14}$ cm^2); N_T ($\times 10^{14}$ cm^{-3}). Note: Ref. 10 does not label the defects with the common nomenclature. The assumptions of *E1* and *E2* in this work are made based on activation temperature and other parameters (E_{CT}, σ_n, and N_T).

Reference	7	8	9	10	14	21	This work
E1	EFG (010): $E_{CT} = 0.56$ EFG ($\bar{2}01$): Not Obs.	EFG (010): $E_{CT} = 0.56$ $\sigma_n = 3$–50	MBE (010): $E_{CT} = 0.56$ $\sigma_n = 3$–50	EFG (010): $E_{CT} = 0.62$ $\sigma_n = 40$ $N_T = 4.7$	HVPE (001): $E_{CT} = 0.6$ $\sigma_n = 0.56$ $N_T = 0.36$	CZ (100): $E_{CT} = 0.55$ $\sigma_n = 0.3$–3 $N_T = 3$–60	EFG ($\bar{2}01$): $E_{CT} = 0.46$ $\sigma_n = 1.6$ $N_T = 90.7$
*E2**	EFG (010), HVPE (001): $E_{CT} = 0.75$, $\sigma_n = 5$	EFG (010), HVPE (001), MBE (010): $E_{CT} = 0.75$ $\sigma_n = 3$–7			HVPE (001): Not Obs.		HVPE (001): $E_{CT} = 0.68$ $\sigma_n = 0.16$ $N_T = 88.5$
E2	All Matls.: $E_{CT} = 0.78$ $\sigma_n = 0.7$	EFG (010): $E_{CT} = 0.78$ $\sigma_n = 0.02$–0.12 MBE (010): Not obs.	HVPE (001): $E_{CT} = 0.78$ $\sigma_n = 0.02$–0.12	EFG (010): $E_{CT} = 0.82$ $\sigma_n = 1$ $N_T = 360$	HVPE (001): $E_{CT} = 0.75$ $\sigma_n = 0.65$ $N_T = 0.46$	CZ (100): $E_{CT} = 0.74$ $\sigma_n = 0.03$–0.3 $N_T = 200$–500	

leakage current. The consequence of investigating defects in leaky devices is that the emission rate e_n is altered with the additional term due to the leakage,[27]

$$e_{n,leaky} = e_n + c_n n = e_n + \frac{J_{leak}\sigma_n}{q}, \tag{5}$$

where $c_n = \sigma_n \nu_{th}$ is the capture coefficient. The consequence of leaky spectra is that the carrier capture cross section, activation energy, and concentration values become inaccurate. For very leaky devices, i.e., where $c_n n$ is comparable to e_n (or possibly greater), the DLTS spectra amplitudes will be reduced. It is rather difficult to discern, from raw DLTS data alone, whether $c_n n$ is a concern or not. Dmowski *et al.*[27] proposed numerical methods to correct for devices with high leakage current, which are not employed here.

Most electrically active defects are formed (and healed) from various thermal processes throughout the lifetime of the crystal; notably, the growth method of the semiconductor crystal has perhaps the most profound impact on its characteristic deep level signatures. Homoepitaxial layers of (100) β-Ga_2O_3 grown by metal organic vapor phase epitaxy (MOVPE) have been shown to suffer from incoherent twin boundaries (ITBs) that manifest as a deep level 0.7–0.8 eV below the conduction band[28] that was otherwise

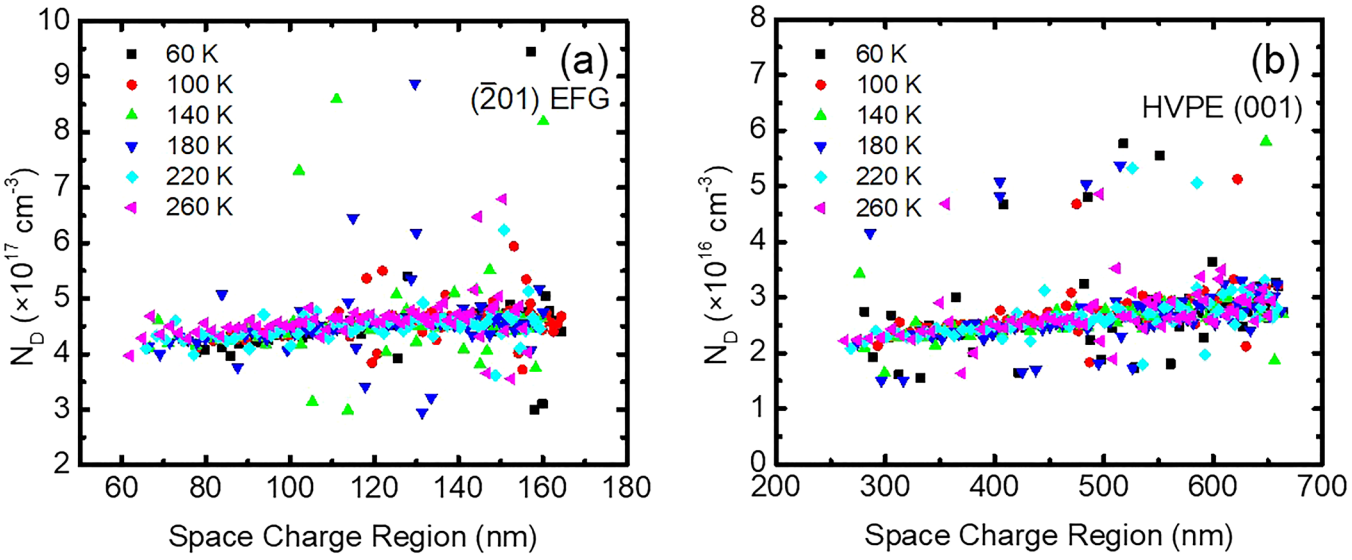

FIG. 8. Doping concentration vs space charge region (SCR) width for the (a) $\bar{2}01$ and (b) (001) samples.

not present in similarly grown (010) samples. Ravadgar *et al.*[29] showed that that low-temperature metal organic chemical vapor deposition (MOCVD) growth of ($\bar{2}01$) β-Ga_2O_3 epilayers resulted in higher surface state densities due to the adsorption of ambient oxygen ions. Post-annealing treatments at 800 °C showed evidence of removing these states. The authors posit that the post-treatment annealing resulted in enough energy for atmospheric oxygen ions to heal oxygen vacancies in the bulk and reduce the electron density, in turn healing the surface states without compromise to the crystal quality.

CONCLUSION

Schottky barrier diodes were designed and fabricated on two different crystal orientations of β-Ga_2O_3: (010) and ($\bar{2}01$) and subjected to DLTS testing. The EFG-fabricated ($\bar{2}01$) material exhibited comparable defect concentrations compared to the HVPE-fabricated (001) sample. Carrier capture cross section and bandgap location of the observed ($\bar{2}01$) defect align well with those of the *E1* defect in recent studies. The epitaxially grown (001) materials demonstrated the presence of what is likely the *E2** defect, contradicting earlier reports of needing low-energy proton radiation to appear in the spectra, methods that were not employed here. Further studies using admittance spectroscopy, a method closely related to DLTS, as well as SIMS, may be fundamental in understanding the nature of these defects and designing future devices.

ACKNOWLEDGMENTS

This work is sponsored by DTRA YIP under Grant HDTRA11710041. The authors gratefully acknowledge the use of facilities within the Eyring Materials Center at Arizona State University. Device fabrication was performed at the Center for Solid State Electronics Research at Arizona State University. Research supported as part of ULTRA, an Energy Frontier Research Center funded by the U.S. Department of Energy (DOE), Office of Science, Basic Energy Sciences (BES), under Award No. DE-SC0021230.

DATA AVAILABILITY

The data that support the findings of this study are available from the corresponding author upon reasonable request.

REFERENCES

[1]H. Xue, Q. He, G. Jian, S. Long, T. Pang, and M. Liu, Nanoscale Res. Lett. **13**, 1 (2018).
[2]S. J. Pearton, J. Yang, P. Cary IV, F. Ren, J. Kim, M. Tadjer, and M. A. Mastro, Appl. Phys. Rev. **5**, 011301 (2018).
[3]J. Montes, C. Yang, H. Fu, T. H. Yang, K. Fu, H. Chen, J. Zhou, X. Huang, and Y. Zhao, Appl. Phys. Lett. **114**, 162103 (2019).
[4]Y. Kwon, G. Lee, S. Oh, J. Kim, S. Pearton, and F. Ren, Appl. Phys. Lett. **110**, 131901 (2017).
[5]J. Kim, S. Oh, M. A. Mastro, and J. Kim, Phys. Chem. Chem. Phys. **18**, 15760 (2016).
[6]Z. Galazka, Semicond. Sci. Technol. **33**, 113001 (2018).
[7]M. E. Ingebrigtsen, J. B. Varley, A. Y. Kuznetsov, B. G. Svensson, G. Alfieri, A. Mihaila, U. Badstübner, and L. Vines, Appl. Phys. Lett. **112**, 042104 (2018).
[8]M. E. Ingebrigtsen, A. Y. Kuznetsov, B. G. Svensson, G. Alfieri, A. Mihaila, U. Badstübner, A. Perron, L. Vines, and J. B. Varley, APL Mater. **7**, 022510 (2019).
[9]M. E. Ingebrigtsen, A. Y. Kuznetsov, B. G. Svensson, G. Alfieri, A. Mihaila, and L. Vines, J. Appl. Phys. **125**, 185706 (2019).
[10]Z. Zhang, E. Farzana, A. R. Arehart, and S. A. Ringel, Appl. Phys. Lett. **108**, 052105 (2016).
[11]H. Ghadi, J. F. McGlone, C. M. Jackson, E. Farzana, Z. Feng, A. F. M. A. U. Bhuiyan, H. Zhao, A. R. Arehart, and S. A. Ringel, APL Mater. **8**, 021111 (2020).
[12]C. Zimmermann, Y. Frodason, A. W. Barnard, J. B. Varley, K. Irmscher, Z. Galazka, A. Karjalainen, W. E. Meyer, F. D. Auret, and L. Vines, Appl. Phys. Lett. **116**, 072101 (2020).
[13]F. Mentink-Vigier, L. Binet, D. Gourier, and H. Vezin, J. Phys. Condens. Matter **25**, 316002 (2013).
[14]A. Y. Polyakov, N. B. Smirnov, I. V. Shchemerov, E. B. Yakimov, J. Yang, F. Ren, G. Yang, J. Kim, A. Kuramata, and S. J. Pearton, Appl. Phys. Lett. **112**, 032107 (2018).
[15]J. E. Hogan, S. W. Kaun, E. Ahmadi, Y. Oshima, and J. S. Speck, Semicond. Sci. Technol. **31**, 065006 (2016).
[16]H. Fu, H. Chen, X. Huang, I. Baranowski, J. Montes, T. H. Yang, and Y. Zhao, IEEE Trans. Electron Devices **65**, 3507 (2018).
[17]A. Broniatowski, Phys. Rev. B **36**, 5895 (1987).
[18]S. Saadaoui, O. Fathallah, and H. Maaref, Mater. Sci. Semicond. Process. **115**, 105100 (2020).
[19]P. Blood and J. Orton, *The Electrical Characterization of Semiconductors: Majority Carriers and Electron States* (Academic Press, San Diego, 1992).
[20]D. V. Lang, J. Appl. Phys. **45**, 3023 (1974).
[21]K. Irmscher, Z. Galazka, M. Pietsch, R. Uecker, and R. Fornari, J. Appl. Phys. **110**, 063720 (2011).
[22]B. Wang, D. Look, and K. Leedy, J. Appl. Phys. **125**, 105103 (2019).
[23]C. A. Lenyk, T. D. Gustafson, L. E. Halliburton, and N. C. Giles, J. Appl. Phys. **126**, 245701 (2019).
[24]S. Bhandari and M. E. Zvanut, J. Appl. Phys. **127**, 065704 (2020).
[25]V. M. Bermudez, Chem. Phys. **323**, 193 (2006).
[26]D. S. Day, M. J. Helix, K. Hess, and B. G. Streetman, Rev. Sci. Instrum. **50**, 1571 (1979).
[27]K. Dmowski, B. Lepley, E. Losson, and M. El. Bouabdellati, J. Appl. Phys. **74**, 3936 (1993).
[28]A. Fiedler, R. Schewski, M. Baldini, Z. Galazka, G. Wagner, M. Albrecht, and K. Irmscher, J. Appl. Phys. **122**, 165701 (2017).
[29]P. Ravadgar, R. -H. Horng, and T. Y. Wang, ECS Trans. **45**, 79 (2012).